J. Fluid Mech. (2010), *vol.* 646, *pp.* 233–253.
doi:10.1017/S0022112009992849

Characterization of the interactions of two unequal co-rotating vortices

LAURA K. BRANDT AND KEIKO K. NOMURA†

Department of Mechanical and Aerospace Engineering, University of California, San Diego, La Jolla, CA 92093-0411, USA

(Received 21 November 2008; revised 16 October 2009; accepted 18 October 2009)

The interactions and merging of two unequal co-rotating vortices in a viscous fluid are investigated. Two-dimensional numerical simulations of initially equal-sized vortices with differing relative strengths are performed. In the case of equal-strength vortices, i.e. symmetric vortex pairs (Brandt & Nomura, *J. Fluid Mech.*, vol. 592, 2007, pp. 413–446), the mutually induced strain deforms and tilts the vortices, which leads to a core detrainment process. The weakened vortices are mutually entrained and rapidly move towards each other as they intertwine and destruct. The flow thereby develops into a single compound vortex. With unequal strengths, i.e. asymmetric pairs, the disparity of the vortices alters the interaction. Merger may result from reciprocal but unequal entrainment, which yields a compound vortex; however other outcomes are possible. The various interactions are classified based on the relative timing of core detrainment and core destruction of the vortices. Through scaling analysis and simulation results, a critical strain rate parameter which characterizes the establishment of core detrainment is identified and determined. The onset of merging is associated with the achievement of the critical strain rate by 'both' vortices, and a merging criterion is thereby developed. In the case of symmetric pairs, the critical strain rate parameter is shown to be related to the critical aspect ratio. In contrast with symmetric merger, which is in essence a flow transformation, asymmetric merger may result in the domination of the stronger vortex because of the unequal deformation rates. If the disparity of the vortex strengths is sufficiently large, the critical strain rate is not attained by the stronger vortex before destruction of the weaker vortex, and the vortices do not merge.

1. Introduction

The merging of two co-rotating vortices is an elementary vortex interaction of both fundamental and practical significance. It plays an important role in the transfer of energy and enstrophy across scales in transitional and turbulent flows. It may also occur in the near-field wake of an aircraft with extended flaps. Yet despite its apparent simplicity and much research, the physical mechanisms of vortex merger have not been fully understood. In the idealized case of 'symmetric' vortex pairs (equal-size and equal-strength vortices), it is known that if the aspect ratio a/b (core size/separation distance) exceeds a critical value, the vortices will merge into a single vortex. What is more commonly observed are 'asymmetric' vortex pairs (unequal-size and/or unequal-strength vortices). In this case, there is greater variation in flow

† Email address for correspondence: knomura@ucsd.edu

behaviour, and the interaction of the vortices may result in the destruction of the smaller and/or weaker vortex. Previous studies of inviscid flow have identified different flow regimes (Dritschel & Waugh 1992; Trieling, Velasco Fuentes & van Heijst 2005). There has been limited consideration of viscous flow. In general, the associated physics are unclear, and a general merging criterion has not been established.

In symmetric vortex merger, two vortices, each with circulation Γ and core size a, separated by a distance b, will rotate about one another because of their mutually induced velocity. In viscous flow, the vortices grow by diffusion, and when a critical aspect ratio $(a/b)_{cr}$ is reached, the vortices move towards each other and develop into a single vortex. The physical mechanisms of this process have been considered in a number of studies (Melander, Zabusky & McWilliams 1988; Meunier 2001; Cerretelli & Williamson 2003; Huang 2005; Velasco Fuentes 2005; Brandt & Nomura 2006, 2007). Melander *et al.* (1988) examined the flow structure in the co-rotating frame of reference which consists of the inner cores, the exchange band and the outer recirculation regions (see figure 4*a*). They indicated that filamentation, which occurs when vorticity enters the outer recirculation regions, modifies the orientation of vorticity contours with respect to the streamlines, and this leads to merger through an inviscid axisymmetrization process. Meunier (2001) and Cerretelli & Williamson (2003) described the merging process in terms of three phases of development, namely diffusive, convective and second diffusive, and associated the onset of merger with the start of the convective phase. They also considered the filaments as the primary driver of convective merger. However, Velasco Fuentes (2005) found that filamentation does not always lead to merger, and in the case of steep vorticity profiles, merger begins before filamentation takes place. Huang (2005) analysed the flow in terms of Lagrangian flow structures and found that both filament and exchange band fluid are responsible for the induced motion of the vortices towards each other.

Recently, Brandt & Nomura (2006, 2007) performed a detailed study of symmetric merger, which clarified the role of filaments and identified the key mechanism involved in the onset of merging. They found that although vorticity associated with filaments acts to advect the vortices towards each other, it does not drive the merger to completion, and in fact the motion may be reversed. The processes of deformation and tilting of the vortices is described in terms of the interaction of vorticity gradient $\nabla\omega$ and rate of strain $\mathbf{S}$. The combined action of tilting and diffusion of vorticity near the centre hyperbolic point, where vorticity is weak, results in the local misalignment of ω and streamlines. This causes vorticity from the core region to enter the exchange band, where it is advected away. The vortex cores are thereby eroded and rapidly move towards each other as they are jointly entrained into the exchange band, whose induced flow becomes dominant and transforms the flow into a single vortex.

In the case of asymmetric co-rotating vortex pairs, there are limited studies (Melander, McWilliams & Zabusky 1987; Dritschel & Waugh 1992; Mitchell & Driscoll 1996; Trieling *et al.* 2005). Melander *et al.* (1987) considered asymmetric merger as an ultimate domination of one of the vortices. Dritschel & Waugh (1992), using detailed contour dynamics simulations, considered the inviscid interactions between two unequal-size vortex patches of uniform and equal vorticity. They classified the interactions into five distinct regimes based on the efficiency of the interaction, defined as the ratio of the final circulation to the initial circulation. 'Elastic interaction' occurs when there are only small deformations and essentially no change in circulation of the vortices. 'Partial straining-out' and 'complete straining-out' regimes are associated with a reduction and a destruction, respectively, of the smaller vortex, with no increase in the larger vortex. 'Complete merger' and 'partial merger'

correspond to increased circulation of the initially larger vortex; i.e. a compound vortex which contains vorticity from both vortices is ultimately formed. A flow regime map, in terms of the initial vortex radii ratio and initial separation distance, is developed. Trieling *et al.* (2005) studied the inviscid interactions of unequal vortices with non-uniform vorticity distributions including a Gaussian profile, which is representative of actual viscous flows. They considered both unequal-size–equal-vorticity and equal-size–unequal-vorticity cases. They found the same flow regimes as those of Dritschel & Waugh (1992) to exist; however the regime boundaries are highly sensitive to the vorticity profile. They showed, through the removal of the low-level vorticity, that it is this 'halo' of low-level vorticity, and not the internal vorticity distribution of the vortex, that causes an increase in the critical distance with decreasing profile steepness. The influence of vorticity distribution was qualitatively similar for both the equal-vorticity and equal-size cases. The resulting mapping of flow regimes is a complex function of vorticity distribution, initial vortex radii ratio (or initial vortex strength ratio) and initial separation distance.

Determination of a merging criterion for symmetric vortex pairs has been the focus of a number of studies (Rossow 1977; Saffman & Szeto 1980; Overman & Zabusky 1982; Griffiths & Hopfinger 1987; Meunier *et al.* 2002). Using contour dynamics of uniform vortices, Saffman & Szeto (1980) and Overman & Zabusky (1982) found a critical separation distance, above which equilibrium configurations of non-circular vortices can exist and below which the vortices are unstable and merge. Ehrenstein & Rossi (1999) and Meunier *et al.* (2002) considered equilibrium states for non-uniform vortices. In these studies, the critical distance is associated with an exchange of stability, which is considered as the onset of merger. The corresponding vortex configuration is characterized by nearly elliptical streamlines within the inner core region and the formation of a cusp at the core outer boundaries in the vicinity of the centre of the pair, where vorticity is low. In the case of an asymmetric vortex pair (Ehrenstein & Rossi 1999), the cusp forms at the outer boundary of the weaker vortex. Meunier *et al.* (2002) developed a general merging criterion for equal non-uniform vortices using both stability analysis and experimental data (viscous flow). The criterion is expressed by a critical aspect ratio with the core size evaluated from the second moment of vorticity (angular impulse). In the experiments, the onset of merging is considered to be the transition from a diffusive-dominated to a convective-dominated process, the former characterized by the diffusive growth of the core. Their results give $(a/b)_{cr} = 0.24 \pm 0.01$. The critical values from their stability analysis are comparable although somewhat lower. They considered these values to differ, since the values are associated with the inception of the instability of an inviscid equilibrium configuration. We note that Brandt & Nomura (2007) determined a critical aspect ratio, associated with the start of the erosion/entrainment process, of $(a/b)_{cr} = 0.235 \pm 0.006$.

In the case of asymmetric merger, Trieling *et al.* (2005) attempted to normalize the separation distance by the second moment of vorticity; however, this does not yield a universal critical aspect ratio which marks the merging flow regimes. With significant asymmetry between vortices, merger may not occur, and the weaker vortex may be strained out and either partially or completely destroyed. Dritschel & Waugh (1992) estimated a critical separation distance for complete destruction of the smaller vortex (i.e. the boundary between partial and complete straining-out) by considering the critical strain rate for an initially circular vortex to undergo irreversible tearing by an imposed adverse shear (Kida 1981; Legras & Dritschel 1993; Mariotti, Legras & Dritschel 1994). This provides a good estimation for the boundary between partial

and complete straining-out regimes in the more asymmetric cases (ratio of initial radii $\lesssim 0.4$). The question that whether a universal critical aspect ratio can be defined for asymmetric merger still remains.

In the present study, we investigate asymmetric co-rotating vortex pairs (equal-size–unequal-strength vortices) in a viscous fluid. Our objectives are to identify the key underlying physical processes involved in the development of the flow and characterize the various flow regimes and vortex interactions. In particular, we establish the conditions for merger. We consider this an important step towards formulating a generalized vortex merging criterion.

We begin with a brief description of the numerical simulations in § 2. Results are presented in terms of basic flow behaviour in § 3, and details of the physical mechanisms are presented in § 4. From this knowledge, we determine a critical strain rate parameter which forms the basis for a merging criterion in § 5. We then formulate a merging criterion and develop a classification of the possible vortex interactions in § 6. The summary and conclusions are given in § 7.

2. Numerical simulations

Two-dimensional numerical simulations of a co-rotating vortex pair are performed for this study. The initial flow field consists of two co-rotating Lamb–Oseen (Gaussian) vortices which are equal in size (same a_o) but differ in strength, with circulation of vortex i, $\Gamma_{i,o}$. The initial flow geometry of the vortex pairs is specified by the aspect ratio a_o/b_o which in these simulations is 0.157, where a_o is defined based on the second moment of vorticity. In the present simulations, the strength of the stronger vortex is fixed and corresponds to a circulation Reynolds number of $Re_{\Gamma,1} = \Gamma_{1,o}/\nu = 5000$. The strength of the weaker vortex varies with respect to the stronger vortex such that the values of the initial circulation ratio $\xi_\Gamma = \Gamma_{2,o}/\Gamma_{1,o}$ considered are $\xi_\Gamma = 1, 0.9, 0.8, 0.7, 0.6, 0.5$ and 0.4. The corresponding range of Re_Γ is comparable to that of the symmetric vortex pair laboratory experiments (Meunier & Leweke 2001) and numerical simulations (Brandt & Nomura 2007) and is moderate in level such that viscous effects are important. We note that the Gaussian vorticity distribution is representative of the initial stages of experimental vortices (Meunier & Leweke 2001; Meunier *et al.* 2002). Based on our symmetric pair simulations, the initial a_o/b_o is such that the vortices are expected to be sufficiently apart and the interaction is established 'naturally' but within a relatively short simulation time. As will be discussed, our analysis of the asymmetric pair (§ 5) provides further considerations for selecting initial conditions for unequal vortices. In general, although the parameter range of our simulations is limited, the results enable us to examine basic aspects of asymmetric vortex interactions.

Numerical simulations were conducted using a pseudo-spectral code with a mixed Crank–Nicolson and third-order Runge–Kutta time-marching scheme with a fixed time step (Bewley 2010, see chapter 13). The computational domain is $L_x = L_z = 12b_o$, with 1024^2 uniform grid points. This allows approximately 27 grid points across the core of each vortex. Periodic boundary conditions are employed in both directions. Domain and resolution tests on both local and integrated quantities show that the domain size and resolution are sufficient. Further discussion of these along with consideration of the boundary conditions are given in Brandt & Nomura (2007).

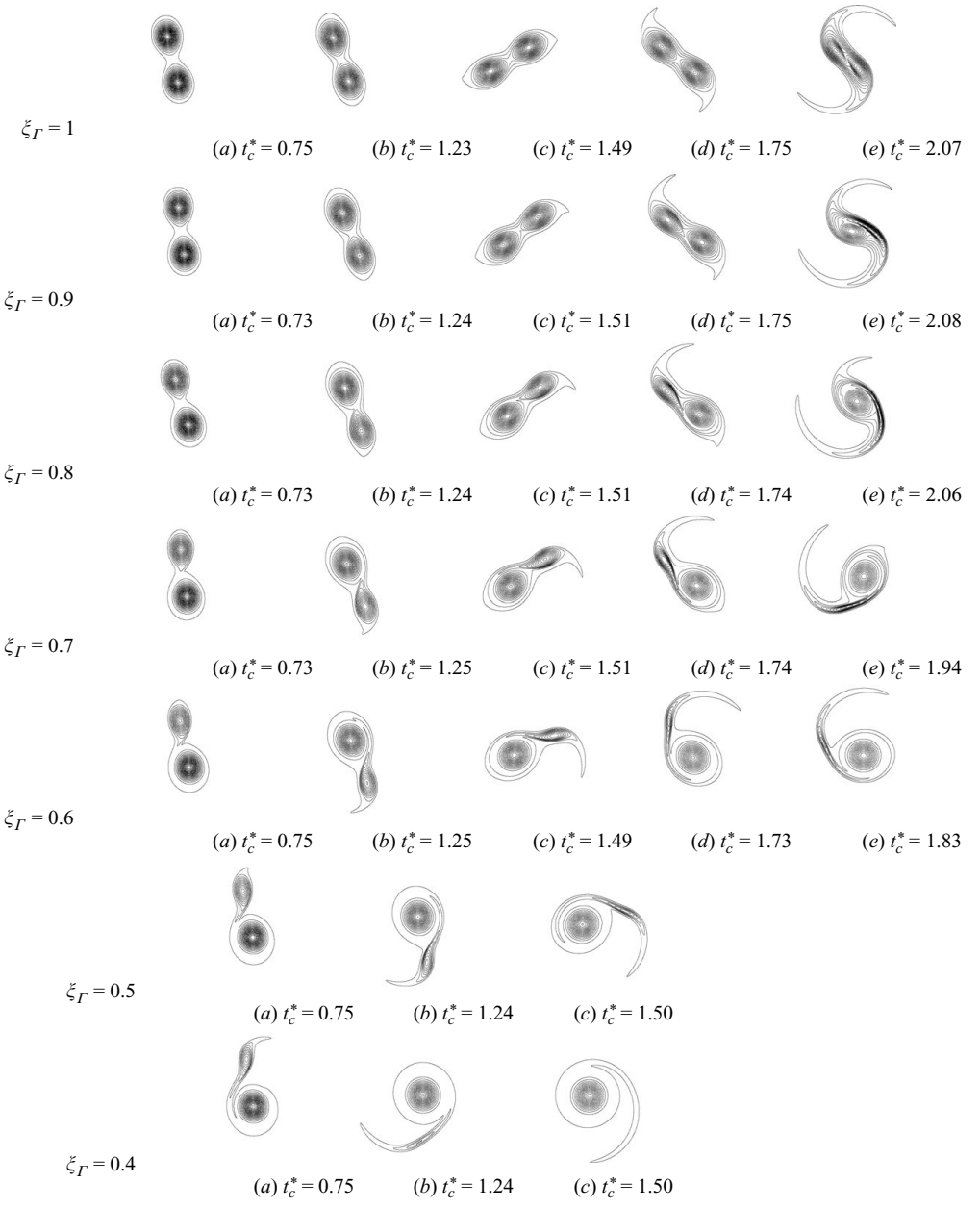

FIGURE 1. Line plots of vorticity contours showing time evolution of flows for different ξ_Γ.

A characteristic convective time scale is the rotational period of a corresponding point vortex system, $T = 2\pi^2 {b_o}^2/\bar{\Gamma}_o$, where $\bar{\Gamma}_o = 0.5(\Gamma_{1,o}+\Gamma_{2,o})$. In the results presented, the non-dimensional time is ${t_c}^* = t/T$.

3. Basic flow development

We begin by examining the basic development of the flows. Figure 1 shows time sequences of vorticity contour plots for different ξ_Γ. Because of the mutually induced

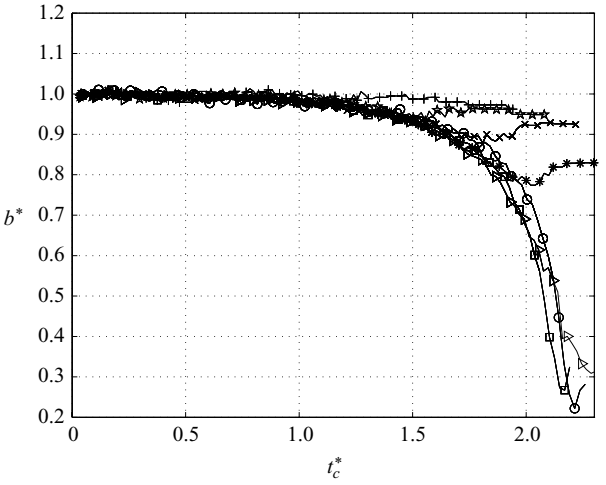

FIGURE 2. Time development of separation distance, $b^*(t) = b(t)/b_o$. Symbols: ○, $\xi_\Gamma = 1$; □, $\xi_\Gamma = 0.9$; ▷, $\xi_\Gamma = 0.8$; *, $\xi_\Gamma = 0.7$; ×, $\xi_\Gamma = 0.6$; ⋆, $\xi_\Gamma = 0.5$; +, $\xi_\Gamma = 0.4$.

velocity, the vortices initially rotate about each other at a relatively fixed distance. The cores grow in time because of diffusion.

In the case of equal vortices ($\xi_\Gamma = 1$; first row in figure 1), the vortex cores deform elliptically as they diffuse. A tilt in the vorticity contours develops near the centre of rotation (CR). Filaments develop at the outer edge of each vortex. The major axes of the vortices are tilted with respect to the connecting line of the vortices; subsequently, the vortices move rapidly towards each other and intertwine. The two vorticity maxima eventually diffuse as the flow evolves towards axisymmetry (not shown).

In the case of unequal vortices ($\xi_\Gamma < 1$), the vortices do not deform at the same rate. As ξ_Γ is reduced, the deformation rate of the weaker vortex becomes increasingly greater in comparison with that of the stronger vortex. The tilt in the weaker vortex develops earlier. For the cases $0.7 \leqslant \xi_\Gamma \leqslant 0.9$, the vortices approach each other; however the stronger vortex appears to endure through the interaction. For $\xi_\Gamma \leqslant 0.6$, the vorticity maxima do not rapidly move towards each other. Instead, the weaker vortex is significantly deformed and becomes encircled about the stronger vortex, eventually diffusing into its low-level outlying vorticity. The stronger-vortex core is relatively unaffected.

Figure 2 shows the time development of non-dimensional separation distance $b^*(t) = b(t)/b_0$, i.e. the distance between the vorticity maxima. In all the flows, $b^*(t)$ remains nearly constant for some time and then exhibits a gradual reduction. As shown in Brandt & Nomura (2007) and indicated in the visualizations (figure 1), the gradual reduction in $b^*(t)$ is associated with the formation of filaments. For $\xi_\Gamma \gtrsim 0.7$, a more rapid reduction in $b^*(t)$ then follows, which occurs at approximately the same time in all the flows. For $\xi_\Gamma \leqslant 0.6$, $b^*(t)$ behaves differently, and beyond the early gradual reduction, it instead exhibits an increase. As will be discussed in § 6, the indicated increase in $b^*(t)$ occurs at times when the weaker vortex is considered to be destroyed. However, for some period of time, vorticity maxima continue to exist, and thus $b^*(t)$ is determined.

With sufficient initial separation, the vortex cores will initially increase in time because of viscous diffusion. There are various ways of defining the size of the vortex

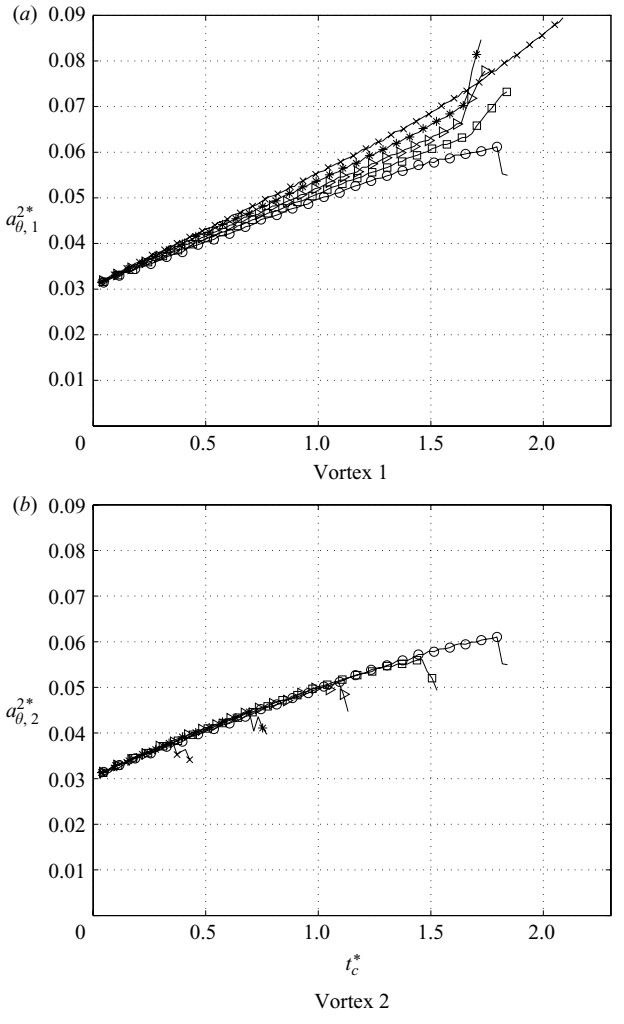

FIGURE 3. Time development of vortex core size, $a^{*2}_{\theta}(t)$. Symbols: ○, $\xi_\Gamma = 1$; □, $\xi_\Gamma = 0.9$; ▷, $\xi_\Gamma = 0.8$; ∗, $\xi_\Gamma = 0.7$; ×, $\xi_\Gamma = 0.6$.

cores to monitor this. Meunier *et al.* (2002) defined the core size by the second moment of vorticity, a_ω. However, in the case of asymmetric vortex pairs, this approach has difficulties, since eventually, vorticity detrained from the weaker vortex is accounted for in the stronger vortex and vice versa. To circumvent this difficulty, we use the (circumferential average) distance between the vorticity maximum and the maximum azimuthal velocity as an indicator of the vortex core size a_θ (Cerretelli & Williamson 2003; Brandt & Nomura 2007). Figure 3 shows $a^{*2}_{\theta} = a^2_\theta / b^2_0$ for both the stronger and weaker vortices. The initial nearly linear development in a^{*2}_{θ} corresponds to growth by viscous diffusion. However, since the vortices also interact and undergo mutual straining during this time, the behaviour of $a^{*2}_{\theta}(t)$ is not strictly linear. In the symmetric case, at some point both cores deviate from their viscous growth. This indicates a transition from a predominantly diffusive-dominated process to a convective-dominated process which corresponds to the primary change in $b^*(t)$. In the asymmetric vortex interactions, the weaker-vortex core (figure 3*b*) deviates

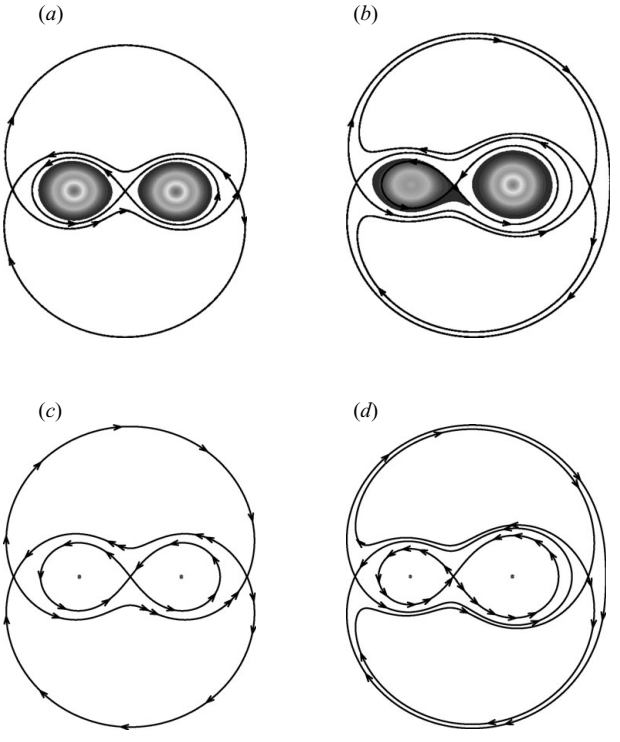

FIGURE 4. Flow structure in the co-rotating frame: (*a*), (*b*) simulation results at $t_c^* = 0.32$; (*c*), (*d*) point vortex system; (*a*), (*c*) $\xi_\Gamma = 1.0$; (*b*), (*d*) $\xi_\Gamma = 0.6$. The streamlines show separatrices of primary flow regions, and the shading corresponds to vorticity.

from its viscous growth earlier in time than the stronger-vortex core. However, this does not cause b^* to rapidly decrease (figure 2). Rather, the rapid decrease in b^* is associated with the departure from viscous growth of the stronger-vortex core. For sufficiently unequal vortices ($\xi_\Gamma \lesssim 0.6$), the latter may not be substantial or may not occur at all (figure 3*a*). In general, the transition from a diffusive-dominated to convective-dominated process, which has been used to determine the critical aspect ratio for symmetric merger (Meunier *et al.* 2002), does not readily yield a corresponding merging criterion for the asymmetric case. In order to develop an appropriate merging criterion, we must gain a better understanding of the physics underlying the vortex interactions.

4. Physical mechanisms

4.1. *Flow structure in the co-rotating frame*

As in previous studies, it is useful to consider the flow in the co-rotating reference frame. Figure 4(*a*, *b*) shows the flow structure for $\xi_\Gamma = 1$ and $\xi_\Gamma = 0.6$ simulation results. Here, the shaded contours indicate vorticity, and the streamlines shown are the separatrices in the co-rotating frame. In figure 4(*c*, *d*), the separatrices are evaluated for a corresponding point vortex system. The basic flow structure is effectively represented by the point vortices as long as the separation is sufficiently large.

In the symmetric vortex pair (figure 4*a*, *c*), there are three primary flow regions. The inner core regions consist of closed streamlines encircling each vorticity maximum.

The exchange band consists of closed streamlines encompassing both the inner core regions. The outer recirculation regions consist of fluid which circulates in the opposite sense (in the co-rotating frame) to that of the cores and exchange band. There are three hyperbolic points in the flow, including the central hyperbolic (CH) point which coincides with the CR.

In the asymmetric vortex pair (figure 4*b*, *d*), the flow structure differs. The locations of the CH point and CR no longer coincide. For a pair of point vortices, the normalized distance between the CR and the centres of the stronger vortex (V1) and weaker vortex (V2), $r^*_{|CR-V1|}$ and $r^*_{|CR-V2|}$ respectively, are given by

$$\left.\begin{aligned} r^*_{|CR-V1|} &= \frac{r_{|CR-V1|}}{b_o} = \frac{\xi_\Gamma}{1+\xi_\Gamma}, \\ r^*_{|CR-V2|} &= \frac{r_{|CR-V2|}}{b_o} = \frac{1}{1+\xi_\Gamma}, \end{aligned}\right\} \tag{4.1}$$

which indicates that the CR is located closer to the stronger vortex as ξ_Γ decreases. We note that in the simulations, the CR remains nearly fixed prior to core destruction. The point vortex system (figure 4*d*) also illustrates the modified flow structure which consists of three hyperbolic points and four primary regions. The inner core and exchange band regions are similar to that of the symmetric case; however, the relative location of the CH point differs. The locations of the three hyperbolic points for the point vortex system are given by

$$(\xi_\Gamma + 1)\, d^{*3}_{|H-V2|} - (\xi_\Gamma + 2)\, d^{*2}_{|H-V2|} - \xi_\Gamma\, d^*_{|H-V2|} + \xi_\Gamma = 0, \tag{4.2}$$

where $d^*_{|H-V2|} = d_{|H-V2|}/b_o$ is the non-dimensional distance from the weaker vortex to a hyperbolic (H) point. Solutions of the cubic equation (4.2) can be determined directly. A fourth-order approximation may also be obtained through a perturbation expansion (with expansion parameter $\sqrt{\xi_\Gamma}$) and provides a simple expression for the location of the CH point,

$$\left.\begin{aligned} d^*_{|CH-V2|} &= \frac{\sqrt{2}}{2}\,{\xi_\Gamma}^{1/2} - \frac{1}{8}\,\xi_\Gamma - \frac{19\sqrt{2}}{128}\,{\xi_\Gamma}^{3/2} + \frac{1}{8}\,{\xi_\Gamma}^2, \\ d^*_{|CH-V1|} &= 1 - d^*_{|CH-V2|}, \end{aligned}\right\} \tag{4.3}$$

which indicates that the smaller the value of ξ_Γ, the closer the CH point is to the weaker vortex. Equation (4.3) provides a good estimate of the initial distance in finite vortices, $D_{2,o} = d_{|CH-V2|,o}$ (to be used in § 5). We note that for very small ξ_Γ, the point vortex approximation breaks down because of the close proximity of the CH point to the finite-size core.

As will be discussed, the processes occurring in the vicinity of the CH point are key in understanding the behaviour of the flow. In the next section, we review the underlying physical processes in the development of the symmetric vortex pair. It is important to understand the key mechanisms involved in vortex merging for this limiting case in which the vortices undergo a fully mutual interaction. We may then consider in § 4.3 the asymmetric vortex pair in which these processes may occur at different times and to varying degrees by each vortex, thereby yielding different flow behaviours.

4.2. *Symmetric vortex interaction and merger*

If the initial vortex separation b_o is sufficiently large, the flow begins its development in a diffusive/deformation phase, associated with constant $b(t)$ and the nearly linear viscous growth of $a^2_\theta(t)$ (figure 3). The mutually induced strain field

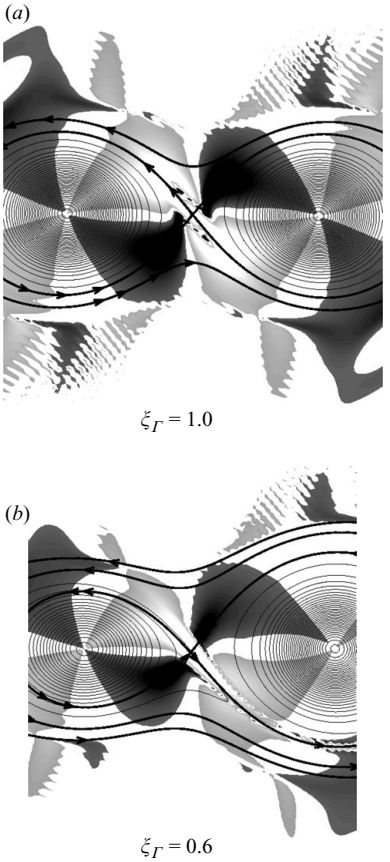

FIGURE 5. The vorticity contours (thin lines) with grey shading corresponding to $\nabla\omega$ production term, $P_s = -(\nabla\omega^T \boldsymbol{S} \nabla\omega)/|\nabla\omega|^2$ (light greyscale denotes $P_s > 0$, and dark greyscale denotes $P_s < 0$), and the instantaneous streamlines (bold lines) in the co-rotating frame at $t_c^* = 0.32$.

establishes the deformation of the vortices which can be described in terms of the interaction of $\nabla\omega$ and $\boldsymbol{S}$ (Brandt & Nomura 2006). Figure 5(a) shows contours of $P_s = -(\nabla\omega^T \boldsymbol{S} \nabla\omega)/|\nabla\omega|^2$ at a relatively early time ($t_c^* = 0.32$). Each vortex exhibits a quadrupole structure of P_s, corresponding to alternate regions of gradient amplification/attenuation by compressive/extensional straining which are associated with the elliptic deformation of the vortices (Kimura & Herring 2001). During this time, the correspondence between ω and the streamfunction is generally maintained, indicating a quasi-equilibrium state (Le Dizes & Verga 2002). However, in the regions of the hyperbolic points where low $|\omega|$ exists, the correspondence begins to deviate. In particular, in the vicinity of the CH point where the induced strain rate is strongest (figure 5a; the light shading near centre corresponds to $P_s > 0$ and high $|P_s|$), the interaction of $\nabla\omega$ and $\boldsymbol{S}$ eventually produces a tilt in ω contours (Brandt & Nomura 2006, 2007).

During the convective/deformation phase, $a_\theta^2(t)$ continues to grow while $b(t)$ gradually decreases. Filamentation is initiated at the outer hyperbolic points. The induced flow by the filaments slowly advects the vortices towards each other. The reduction in $b(t)$ enhances the induced $\boldsymbol{S}$ at the CH point. The enhanced tilting of ω in the vicinity of the CH point causes ω from the core regions to enter the

exchange band, where it is advected away. We consider the establishment of this core detrainment process to be the predominant cause of departure from quasi-equilibrium, diffusion-dominated conditions to convective-dominated conditions.

In the convective/entrainment phase, the vortex cores erode significantly, which disrupts the diffusive growth of $a_\theta^2(t)$. At some point, the integrity of the vortices is sufficiently diminished. The cores are then entrained into the exchange band (they are essentially mutually entrained), whose induced flow becomes dominant. The original vortices are destroyed as the flow transforms into a single compound vortex. This corresponds to the rapid reduction in $b(t)$. A critical aspect ratio, associated with the start of the convective/entrainment phase, is determined for a range of flow conditions: $(a/b)_{cr} = 0.235 \pm 0.006$ (Brandt & Nomura 2007). It is also noted that this time is comparable to the time $a^2(t)$ (and $a_\theta^2(t)$) deviates from its viscous growth.

4.3. *Asymmetric vortex interactions*

In the case of the asymmetric vortex pair, the difference in vortex strengths alters the flow structure and interaction. The variation in local time scales may be such that the vortices no longer experience the flow processes simultaneously.

Initially the two vortices will develop in a diffusive/deformation phase in which both cores grow by diffusion (figure 3). However, the greater deformation rates at the weaker vortex will cause an earlier departure of it from this phase. A measure of the rate of vortex deformation is the local eccentricity ϵ_l defined as the ratio of the strain rate to the rotation rate (Le Dizes & Verga 2002). Figure 6 shows ϵ_l evaluated at the vorticity maximum of each vortex. The results clearly indicate the disparity in deformation rates between the vortices. We note that for $\xi_\Gamma \leqslant 0.6$, the local eccentricity of the stronger vortex, $\epsilon_{l,1}$, remains low and, in time, indicates little influence by the weaker vortex. The implication of the differences in deformation rates is indicated in figure 5(*b*): P_s is stronger at the weaker vortex because of the $\boldsymbol{S}$ induced by the stronger vortex; conversely, P_s is weaker at the stronger vortex because of the $\boldsymbol{S}$ induced by the weaker vortex. As discussed in § 4.1, the CH point is closer to the weaker vortex. The weaker vortex is thereby subject to earlier tilting in the vicinity of the CH point and the resultant core detrainment.

As discussed, in the symmetric vortex pair, a convective/deformation phase follows in which there is a gradual motion of the vortices towards each other because of the induced flow by the filaments. As seen in figure 2, this occurs at approximately $t_c^* \sim 1$ (approximately one revolution of the vortex pair) for all ξ_Γ considered. After this time, filaments are observed in the flows (figure 1). However, the more asymmetric the vortex pair is, the more the filamentation that occurs on the weaker-vortex side. Filamentation occurs when ω from the core and exchange band enters the outer-recirculation regions because of the combined action of diffusion and tilting of ω contours in the vicinity of the outer hyperbolic points (figure 4). Once ω enters the outer-recirculation region, it is advected away by the flow in this region, thereby forming filaments. As noted in § 4.1, the asymmetric pair contains an additional region just outside the exchange band on the outer side of the stronger vortex (figure 4*b*,*d*). This acts to buffer the stronger vortex from the nearby outer hyperbolic point. Any ω diffusing out from the exchange band in this region will be advected into the filament of the weaker vortex. This change in the flow structure assists the stronger vortex to retain its shape. In contrast, the enhanced filamentation occurring on the side of the weaker vortex further promotes the deformation and erosion of the weaker vortex.

Although the weaker vortex experiences significant erosion, as indicated by its departure from viscous core growth $a_{\theta,2}^2(t)$ (figure 3*b*), and ω is entrained into the

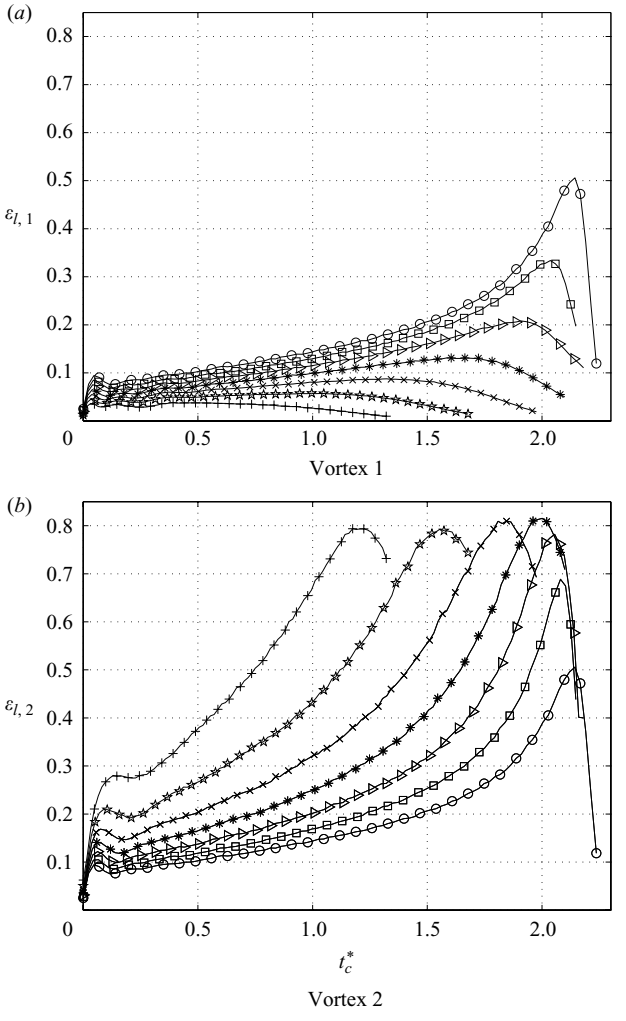

FIGURE 6. Time development of the local eccentricity for each vortex. Symbols: ○, $\xi_\Gamma = 1$; □, $\xi_\Gamma = 0.9$; ▷, $\xi_\Gamma = 0.8$; *, $\xi_\Gamma = 0.7$; ×, $\xi_\Gamma = 0.6$; ⋆, $\xi_\Gamma = 0.5$; +, $\xi_\Gamma = 0.4$.

exchange band, $b(t)$ does not correspondingly exhibit a significant decrease (figure 2). This may be understood by considering the results of Huang (2005), who used a vortex simulation method to track Lagrangian flow structures in a symmetric vortex pair. It is shown that the primary inward motion of a given ('computed') vortex is due to a 'sheet-like' structure emitted by the opposite ('imaged') vortex as it wraps around the computed vortex (see figure 7 in Huang 2005). That is to say as a vortex is detrained, its $\boldsymbol{\omega}$ is entrained into the exchange band and advected around the companion vortex; the induced velocity moves the companion towards it. In the symmetric case, this process is reciprocal and equal and results in the mutual entrainment of the cores into each other and intertwinement. In the case of the asymmetric vortex pair, the weaker vortex erodes earlier in time. The relatively weak detrained $\boldsymbol{\omega}$ may advect around the stronger vortex; however the associated induced flow on the stronger vortex is correspondingly weak and insufficient to result in significant motion.

If, within some time period, the stronger vortex also erodes sufficiently, then there will be some extent of mutual (reciprocal), but unequal, entrainment. This is observed

in the simulations with $0.7 \leqslant \xi_\Gamma \leqslant 0.9$, where it is seen that the viscous growth of the stronger core, $a^2_{\theta,1}(t)$, is eventually interrupted (figure 3*a*). However in these cases, the stronger vortex ultimately dominates (figure 1) and entrains $\boldsymbol{\omega}$ from the weaker vortex. We therefore consider the process as vortex 'merger', since the result is an enhanced (compound) vortex. If significant erosion occurs in the weaker vortex before it is established in the stronger vortex (e.g. $\xi_\Gamma = 0.6$), the weaker vortex is destroyed, leaving the stronger vortex to remain in the flow relatively unaffected, since there is no longer a significant source of external strain to deform it and initiate erosion. In this case, merger does not occur.

We therefore consider a critical state for a given vortex to be associated with the establishment of core detrainment. If both vortices attain this state, there will be some degree of mutual entrainment (intertwinement) which results in an enhanced vortex; i.e. convective merger will occur. Based on these ideas, we may now consider the development of a merging criterion.

5. Critical strain rate parameter

From our analysis of the physics, a simple mean critical aspect ratio, $(1/2)((a_1 + a_2)/b)$, is not expected to appropriately characterize the onset of merger in asymmetric vortex pairs, and an alternative criterion is needed. As discussed above, we consider a critical state of a given vortex to be associated with the establishment of core detrainment. Since the process is initiated by the interaction between $\boldsymbol{S}$ and $\nabla\omega$ in the vicinity of the CH point, we expect that it will proceed if the induced local strain rates are sufficiently high. We therefore consider one characteristic quantity to be the strain rate at the CH point, S_{CH}. Furthermore, we expect significant core detrainment to occur if the vortex strength is relatively weak. A characteristic core vorticity is the maximum, ω_{v_i}. In order to relate the strain rate at the CH point, which has contributions from both vortices, to the maximum vorticity of the vortex, we normalize each quantity by a characteristic local strain rate,

$$S^*_{CH} = \frac{S_{CH}}{S_{CH,o}}, \quad \omega^*_{v_i} = \frac{\omega_{v_i}}{S_{v_i,o}}, \tag{5.1}$$

where $S_{CH,o}$ and $S_{v_i,o}$ are the initial strain rates at the CH and vorticity maximum points, respectively. This introduces appropriate scaling for these quantities. We may then define a strain rate parameter for vortex i,

$$\gamma_i(t) \equiv \left(\frac{S^*_{CH}(t)}{\frac{1}{2}\omega^*_{v_i}(t)} \right)^{1/2}, \tag{5.2}$$

which is a measure of the relative strength of the induced strain rate at the CH point to the vortex strength. Figure 7 shows computed $\gamma_1(t)$ and $\gamma_2(t)$ from the simulations. We then consider the critical value of the vortex strain rate parameter to be the value at the critical time $t_{cr,i}$ when core detrainment is established, i.e. $\gamma_{cr,2} = \gamma_2(t_{cr,2})$ and $\gamma_{cr,1} = \gamma_1(t_{cr,1})$. As discussed in the previous section, this also corresponds to the time at which the departure from viscous core growth occurs for the given vortex. Thus, $t_{cr,i}$ can be determined from figure 3 ($a^{*2}_\theta(t)$). Then, at these corresponding times, we determine from figure 7 for the weaker and stronger vortices, respectively, $\gamma_{cr,2} = 0.245 \pm 0.005$ and $\gamma_{cr,1} = 0.249 \pm 0.003$. The two values are within the range of

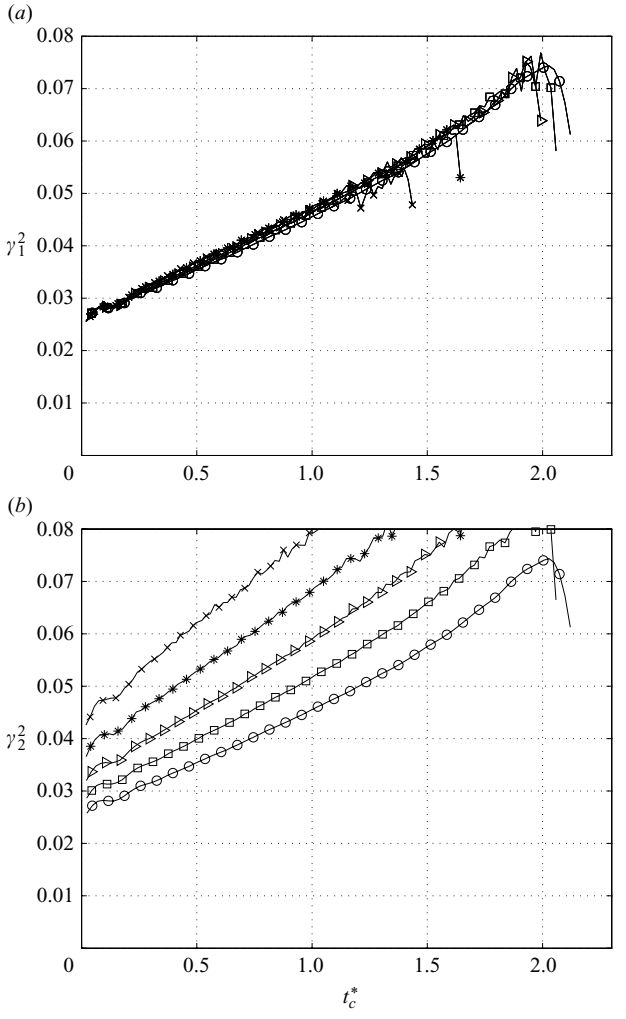

FIGURE 7. Time development of the strain parameter γ_i for (a) vortex 1 and (b) vortex 2. Symbols: ○, $\xi_\Gamma = 1$; □, $\xi_\Gamma = 0.9$; ▷, $\xi_\Gamma = 0.8$; *, $\xi_\Gamma = 0.7$; ×, $\xi_\Gamma = 0.6$.

their variations. We therefore find a 'single value for the critical strain rate parameter',

$$\gamma_{cr,1} \approx \gamma_{cr,2} \approx \gamma_{cr} = 0.247 \pm 0.007. \tag{5.3}$$

As a rudimentary test for the generality of (5.3), some additional simulations were performed with other parameter values ($Re_{\Gamma,i}$, a_o/b_o, $a_{2,o}/a_{1,o}$). Resulting values for γ_{cr} are within the range given in (5.3). We note that data for cases in which the simulation initial flow condition are near or beyond the critical state, e.g. $\xi_\Gamma \lesssim 0.5$, is excluded from (5.3), as will be discussed below. Regarding the sensitivity of the evaluation of $\gamma_{cr,i}$ to the determination of the CH point, since the flow is unsteady, the changing angular velocity makes precise determination of the CH point somewhat difficult. To examine this sensitivity, $\gamma_{cr,i}$ was determined within a region surrounding the CH point of 9×9 grid points. The range of values found are $\gamma_{cr,1} = 0.249 \pm 0.005$, $\gamma_{cr,2} = 0.243 \pm 0.006$ and $\gamma_{cr} = 0.246 \pm 0.008$. Thus, errors in determining the exact location of the CH

point (within a distance of approximately $0.3a_o/b_o$) may introduce errors in the strain rate parameter value of 2–3 % for the flow conditions considered.

We now further consider the strain rate parameter, in particular that of the weaker vortex γ_2, through a scaling analysis. Prior to significant vortex interaction, S_{CH} is proportional to the local external strain rate which depends on the distance between the vortices and CH point, $D_i = d_{|CH-V_i|}$, and ω_{v_i} is proportional to the ratio of Γ_i and $a_{\omega,i}^2$,

$$S_{CH} \propto \frac{\Gamma_1}{2\pi D_1^2} + \frac{\Gamma_2}{2\pi D_2^2}, \qquad \omega_{v_i} \propto \frac{\Gamma_i}{\pi a_{\omega,i}^2}. \tag{5.4}$$

We thereby have the following scaling for the non-dimensional strain rate and vorticity:

$$\left.\begin{aligned} S_{CH}^* = \frac{S_{CH}}{S_{CH,o}} &\propto \left[\frac{\Gamma_2}{\Gamma_{2,o}}\right]\left[\frac{D_{2,o}^2}{D_2^2}\right]\left[\frac{1+\dfrac{1}{\xi_\Gamma}\dfrac{D_2^2}{D_1^2}}{1+\dfrac{1}{\xi_\Gamma}\dfrac{D_{2,o}^2}{D_{1,o}^2}}\right], \\ \omega_{v_i}^* = \frac{\omega_{v_i}}{S_{v_i,o}} &\propto \left[\frac{\Gamma_i}{\Gamma_{1,o}}\right]\left[\frac{2}{a_{\omega,i}^{*2}}\right]. \end{aligned}\right\} \tag{5.5}$$

Note that in the equations above, the approximation that $\Gamma_2/\Gamma_1 \approx \Gamma_{2,o}/\Gamma_{1,o} = \xi_\Gamma$ was made. This relationship, as well as the scaling in (5.4), holds reasonably well up to the critical state of the weaker vortex. The strain rate parameter for the weaker vortex, γ_2, may then be related to ξ_Γ along with a_ω and D_i,

$$\gamma_2(t) \equiv \left(\frac{S_{CH}^*}{\frac{1}{2}\omega_{v_2}^*}\right)^{1/2} = \left(\left[\frac{S_{CH}}{\frac{1}{2}\omega_{v_2}}\right]\left[\frac{D_{2,o}^2}{\xi_\Gamma}\right]\left[\frac{1}{1+\dfrac{1}{\xi_\Gamma}\dfrac{D_{2,o}^2}{D_{1,o}^2}}\right]\right)^{1/2} \tag{5.6}$$

$$\propto a_{\omega,2}^*\, {\xi_\Gamma}^{-1/2}\left[\frac{D_{2,o}}{D_2}\right]\left(\frac{1+\dfrac{1}{\xi_\Gamma}\dfrac{D_2^2}{D_1^2}}{1+\dfrac{1}{\xi_\Gamma}\dfrac{D_{2,o}^2}{D_{1,o}^2}}\right)^{1/2}. \tag{5.7}$$

This gives the following scaling for γ_{cr} for the weaker vortex:

$$\gamma_{cr,2} = f\, a_{\omega,2}^*(t_{cr,2}^*){\xi_\Gamma}^{-1/2}\left[\frac{D_{2,o}^2}{D_2^2(t_{cr,2}^*)}\right]\left(\frac{1+\dfrac{1}{\xi_\Gamma}\dfrac{D_2^2(t_{cr,2}^*)}{D_1^2(t_{cr,2}^*)}}{1+\dfrac{1}{\xi_\Gamma}\dfrac{D_{2,o}^2}{D_{1,o}^2}}\right)^{1/2}, \tag{5.8}$$

where f is a proportionality constant. From the simulation results for the weaker vortex ($\gamma_{cr,2} = 0.245 \pm 0.005$) and (5.8), the proportionality factor is found to be $f = 1.05 \pm 0.03$. In the case of a 'symmetric vortex pair' ($\xi_\Gamma = 1$), (5.8) reduces to

$$\gamma_{cr,2} = \left(\frac{S_{CH}^*(t_{crit}^*)}{\frac{1}{2}\omega_{v_2}^*(t_{crit}^*)}\right)^{1/2} = \left(\frac{S_{CH}(t_{crit}^*)}{4\omega_{v_i}(t_{crit}^*)}\right)^{1/2} = f\,\frac{a_\omega^*(t_{crit}^*)}{2\,D(t_{crit}^*)} = f\left(\frac{a_\omega}{b}\right)_{crit}. \tag{5.9}$$

Thus in this case, $\gamma_{cr,2} = \gamma_{cr,1} = \gamma_{cr}$ is directly related to the critical aspect ratio $(a_\omega/b)_{crit}$. From the results indicated above, $\gamma_{cr,2}/f = 0.233 \pm 0.005$. This can be compared with our previous results for symmetric merger, $(a_\omega/b)_{crit} = 0.235 \pm 0.006$ (Brandt & Nomura 2007). The good agreement demonstrates the relation in (5.9) and our determined value for f.

We note that a corresponding scaling analysis (5.8) for the stronger-vortex critical strain rate $\gamma_{cr,1}$ may not be carried out. In general, when (if) the stronger vortex reaches the critical state, significant changes may have occurred for the weaker vortex, and the associated strain field and scaling for S_{CH} are no longer straightforward. We also noted earlier that data for $\xi_\Gamma \lesssim 0.5$ are not included in the determination of $\gamma_{cr,i}$ in (5.3). Recall that for lower ξ_Γ, the CH point is closer to the weaker vortex (4.3). From (5.6) and (4.3), the weaker-vortex core size for $\xi_\Gamma = 0.5$ is $a^*_{\omega,2}(t^*_{cr,2}) \approx 0.163$, which is close to the initial value of $a^*_o = 0.157$ (initial aspect ratio). Therefore, for $a_{\omega,o}/b_o = 0.157$ and $\xi_\Gamma \lesssim 0.5$, the weaker vortex is already close to or beyond the critical state and is quickly destroyed. This gives more precise limitations on the initial conditions for the simulations than discussed in § 2.

As discussed in § 4.3, for an asymmetric vortex pair, convective merger will occur if both vortices reach the critical state. The critical state of the weaker vortex is achieved earlier, when $\gamma_2(t) = \gamma_{cr,2}$. From figure 7(*b*) it is observed that $\gamma_1(t)$ eventually reaches its critical value for $\xi_\Gamma \gtrsim 0.7$. However, in the case of $\xi_\Gamma = 0.6$, $\gamma_1(t)$ does not achieve the critical value, and correspondingly, $a_{\theta,1}$ does not deviate from viscous growth (figure 3*a*). Core detrainment is not established by the stronger vortex, and convective merger does not occur in this case.

6. Merging criterion and classification of vortex interactions

In our viscous flow simulations in § 4.3, several distinct vortex interactions/flow regimes are observed for the asymmetric pair. We may characterize these interactions, and in particular merger, based on the timing of key processes: weaker-vortex core detrainment, stronger-vortex core detrainment and weaker-vortex destruction. Figure 8 shows these process times (scaled by convective time scale) as a function of ξ_Γ. The observed interactions may be identified in terms of the relative timing of these processes. We first consider each of the times separately.

The time required for the weaker vortex to reach the critical state ($\gamma_2(t) = \gamma_{cr}$), $t^*_{cr,2}$ (□ in figure 8), is seen to increase linearly with respect to ξ_Γ. As stated earlier, $t^*_{cr,2}$ is evaluated in the simulations as the time of departure from viscous core growth. Based on the scaling analysis in the previous section (§ 5), $t^*_{cr,2}$ can then be estimated through the right-hand side of (5.8) and assuming a linear viscous growth relation for $a_\omega(t)$,

$$a^2_{\omega,2} = c^2_{\omega,2}\, \nu\, t + a^2_{\omega,o}. \tag{6.1}$$

For symmetric vortex pairs, Brandt & Nomura (2007) found $c_\omega = 2.11$ for all cases considered, and the behaviour is similar to that of a single vortex. However, in the asymmetric vortex pairs, the weaker-vortex core growth differs (figure 3*b*), and the growth rate is found to scale with the rotation rate $c^2_{\omega,2} = 2.11^2\sqrt{.5(1+\xi_\Gamma)}$. From (5.8), the resulting equation is of the form

$$t^*_{cr,2} \approx \left(\left[\frac{\gamma^2_{cr}}{f^2} \right] \left[\frac{Re_{\Gamma,2}}{4\, c^2_{\omega,2}\, \pi^2} \right] g - \left[\frac{a^{*2}_{\omega,o} Re_{\Gamma,1}}{4\, c^2_{\omega,2}\, \pi^2} \right] \right) \left[1 + \xi_\Gamma \right], \tag{6.2}$$

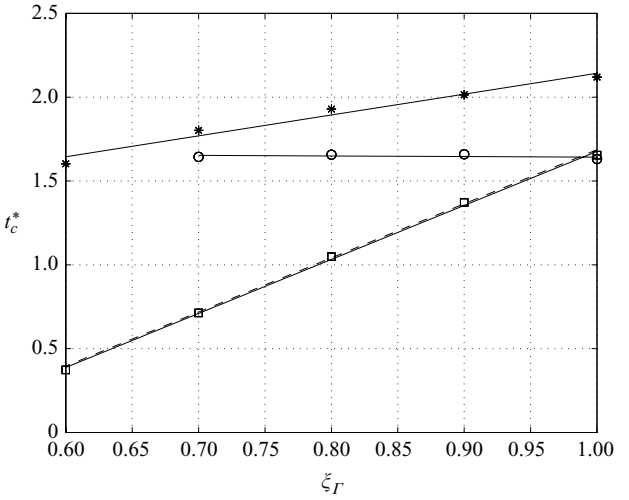

FIGURE 8. Process times (scaled by convective time scale) corresponding to weaker-vortex detrainment ($t^*_{cr,2}$, □), stronger-vortex detrainment ($t^*_{cr,1}$, ○) and weaker-vortex destruction ($t^*_{de,2}$, ∗). The dashed line corresponds to (6.2).

where the factor g is given by

$$g = \left[\frac{D_2^2(t^*_{cr,2})}{D_{2,o}^2}\right]\left[\frac{1+\dfrac{1}{\xi_\Gamma}\dfrac{D_{2,o}^2}{D_{1,o}^2}}{1+\dfrac{1}{\xi_\Gamma}\dfrac{D_2^2(t^*_{cr,2})}{D_1^2(t^*_{cr,2})}}\right]. \tag{6.3}$$

In general, the precise behaviours of $D_1(t)$ and $D_2(t)$ are complex. However, prior to detrainment of the weaker vortex, the CH point is not significantly altered by changes in the flow field. Evaluation of g (6.3) using $D_1(t^*_{cr,2})$ and $D_2(t^*_{cr,2})$ from the simulations gives $g = 0.985 \pm 0.008$, which indicates that this parameter may be considered approximately constant for the cases considered. After detrainment of the weaker vortex is established, the hyperbolic points begin to significantly shift, and this approximation becomes invalid. Using this approximation in (6.2) gives the resulting prediction for $t^*_{cr,2}$, which is represented by the dashed line in figure 8. As indicated, the relation effectively predicts the time for weaker-vortex core detrainment. This also corroborates our scaling analysis in § 5.

The time at which the stronger vortex reaches the critical state, $t^*_{cr,1}$ (○ in figure 8), appears to be independent of ξ_Γ. Therefore, this critical time may be defined based on the case of symmetric merger. Using (5.9) and (6.1), we obtain

$$t^*_{cr,1} = [Re_{\Gamma,1} + Re_{\Gamma,2}]\left[\frac{a^{*2}_{\omega,1} - a^{*2}_{\omega,o}}{4\,c^2_{\omega,1}\pi^2}\right] \approx Re_{\Gamma,1}\frac{(\gamma_{cr}/f)^2\,b^{*2}_{sym} - a^{*2}_{\omega,o}}{2\,c^2_{sym}\pi^2}. \tag{6.4}$$

For our simulation flow conditions, $t^*_{cr,1} = 1.65 \pm 0.02$. We note that unlike the weaker vortex, the stronger-vortex core growth is not dependent on rotation rate and $c_{\omega,1} \approx 2.11$.

The final process time considered is the time characterizing the destruction of the weaker vortex, $t^*_{de,2}$ (∗ in figure 8). In the present analysis, the weaker vortex is considered to be destroyed when its core vorticity no longer dominates over the

imposed strain rate field. An indicator of this is the second invariant of the velocity gradient tensor, $II = (\boldsymbol{\omega}^2/2 - \boldsymbol{S}^2)/2$. Thus, we estimate the destruction time $t^*_{de,2}$ when the local value of II at the vorticity maximum, II_{V2}, is very small. The values shown in figure 8 correspond to $II_{V2} = 0.05\, II_{V1,0}$. Although this is a highly simplified characterization of vortex destruction, it serves the purposes of the present analysis. Other flow characteristics, e.g. $b^*(t)$ (figure 2, $\xi_\Gamma \leqslant 0.7$), also indicate that the flow is significantly altered around the time, $t^* = t^*_{de,2}$.

We now formulate a classification scheme for the observed vortex interactions in § 4.3. We consider the classifications previously developed for inviscid asymmetric vortex interactions (Dritschel & Waugh 1992; Trieling *et al.* 2005). However, here we modify the definitions for viscous flow. Based on our analysis, we classify our simulations in terms of three interactions: complete merger, partial merger and straining-out. These are characterized as follows.

(i) Complete merger ($\xi_\Gamma = 1.0$ in present simulations): detrainment from both vortices; mutual entrainment of the cores transforms the flow into a single vortex,

$$t^*_{cr,2} \approx t^*_{cr,1} < t^*_{de,2}. \tag{6.5}$$

(ii) Partial merger ($\xi_\Gamma = 0.9, 0.8, 0.7$): detrainment from both vortices; weaker vortex is destroyed and entrained by the stronger vortex,

$$t^*_{cr,2} < t^*_{cr,1} < t^*_{de,2}. \tag{6.6}$$

(iii) Straining-out ($\xi_\Gamma \leqslant 0.6$): detrainment from weaker vortex only; weaker vortex is destroyed,

$$t^*_{cr,2} < t^*_{de,2} < t^*_{cr,1}. \tag{6.7}$$

These interactions all eventually result in a single vortex for which the circulation may differ from that of the initial vortices. In complete merger, the circulation of the final compound vortex is greater than that of either original vortex. This increase is due to the mutual entrainment of both vortices and the transformation into a single vortex. The concept of partial merger in a viscous fluid is not as clear as in inviscid interactions. In the cases considered, vorticity is detrained from both vortices; however, the weaker vortex is destroyed before the stronger vortex is significantly eroded. Ultimately, the stronger vortex dominates and is enhanced by the entrained vorticity from the weaker vortex. The interaction thus still yields a compound vortex with increased circulation. In the flows in which the weaker vortex is strained out, there is no mutual entrainment. The stronger vortex remains, but its circulation may not be significantly changed. These interactions do not yield a compound vortex, and thus merger does not occur.

7. Conclusions

The interaction of two unequal co-rotating vortices in a viscous fluid has been investigated using two-dimensional numerical simulations. The vortices considered have the same initial core size and different strengths. In the simulations presented, the initial aspect ratio is fixed at $a_0/b_0 = 0.157$. The initial strength of the stronger vortex is given by $Re_{\Gamma,1} = 5000$, and the range of values of the initial circulation ratio considered is $0.4 \leqslant \xi_\Gamma \leqslant 1.0$. Although the parameter range of our simulations is limited, the results reveal the basic aspects of asymmetric vortex interactions.

The primary physical mechanisms involved in the vortex interactions and development of the flow are identified and described. As in symmetric vortex pairs,

the vortices initially grow by diffusion. In the vicinity of the CH point, the interaction of $\nabla\omega$ and induced $\boldsymbol{S}$ may produce a tilt in ω contours, which causes ω from the core region to enter the exchange band, thereby initiating core detrainment. In the asymmetric pair, the deformation rates are stronger at the weaker vortex because of the difference in induced $\boldsymbol{S}$, and the tilt of ω contours and subsequent core detrainment occur earlier than the stronger vortex. However, the dominant attracting motion occurs only when, and if, core detrainment is established by the stronger vortex. If this occurs, then there will be some extent of mutual (reciprocal) but unequal entrainment. This intertwinement is needed for merging and is observed in the present simulations ($a_0/b_0 = 0.157$, $Re_{\Gamma,1} = 5000$) for $0.7 \leqslant \xi_\Gamma \leqslant 0.9$. However in these cases, the stronger vortex ultimately dominates and entrains vorticity from the weaker vortex. We therefore consider the process as vortex 'merger', since the result is an enhanced compound vortex. If core detrainment is not established by the stronger vortex before significant erosion occurs in the weaker vortex ($\xi_\Gamma \leqslant 0.6$), the weaker vortex is destroyed, leaving the stronger vortex to remain in the flow relatively unaffected. In this case, merger does not occur.

Knowledge of the key underlying processes enables the development of a basis for a merging criterion for unequal vortices. We consider the critical state for a given vortex to be associated with the establishment of core detrainment. A vortex strain rate parameter, γ_i, is defined in terms of the ratio of the strain rate at the CH point, S_{CH}, to the maximum vorticity of vortex i, ω_{v_i}, thereby providing a measure of the relative strength of the induced strain rate at the CH point to the vortex strength. We then consider the critical value of γ_i to be the value at the critical time, $t_{cr,i}$, when core detrainment (and entrainment into exchange band) is established, i.e. $\gamma_{cr,2} = \gamma_2(t_{cr,2})$ and $\gamma_{cr,1} = \gamma_1(t_{cr,1})$. The onset of merging is associated with the joint achievement of the critical strain rate by both vortices. For all our simulations, we find a single critical value for both vortices, i.e. $\gamma_{cr,1} = \gamma_{cr,2} = \gamma_{cr} = 0.247 \pm 0.007$. In the case of equal vortices, the critical strain rate is shown to be related to the critical aspect ratio (5.9). From the present results, $\gamma_{cr,2}/f = 0.233 \pm 0.005$, which compares well with the previously determined values for the critical aspect ratio for symmetric vortex merger, $(a_\omega/b)_{crit} = 0.235 \pm 0.006$ (Brandt & Nomura 2007).

From our viscous flow simulations, three distinct vortex interactions are observed. We define the interactions based on modifications of the classifications previously developed for inviscid asymmetric vortex interactions (Dritschel & Waugh 1992; Trieling *et al.* 2005). However, here we characterize the interactions based on the relative timing of key processes: weaker-vortex core detrainment ($t_{cr,2}$), stronger-vortex core detrainment ($t_{cr,1}$) and weaker-vortex destruction ($t_{de,2}$). We consider 'complete merger' to occur if both vortices reach γ_{cr} and are mutually entrained prior to vortex destruction ($t^*_{cr,2} \sim t^*_{cr,1} < t^*_{de,2}$). The flow is transformed into a single compound vortex in which the final circulation is increased because of the contribution of both vortices. We consider 'partial merger' to occur when both vortices reach γ_{cr}; however, the weaker vortex is destroyed before the stronger vortex is significantly eroded ($t^*_{cr,2} < t^*_{cr,1} < t^*_{de,2}$). Ultimately, the stronger vortex dominates and is enhanced by the entrained vorticity from the weaker vortex. The interaction thus yields a compound vortex with increased circulation. We consider flows in which the weaker vortex is 'straining out' when only the weaker-vortex core is detrained and destroyed ($t^*_{cr,2} < t^*_{de,2} < t^*_{cr,1}$). There is no mutual entrainment. The stronger vortex remains, but its circulation may not be significantly altered. These interactions do not yield a compound vortex, and thus merger does not occur.

In conclusion, we have developed a description of asymmetric vortex interactions for viscous flow and, in particular, a more general criterion for vortex merger, i.e. $t^*_{cr,2} \leqslant t^*_{cr,1} < t^*_{de,2}$. While this specifies the required conditions for merging, our results do not yet enable the prediction of the outcome for a given initial vortex pair. In the case of symmetric pairs in viscous fluid, $t^*_{cr,2} = t^*_{cr,1} = t^*_{cr}$, and since $t^*_{cr} < t^*_{de}$ will always be the case (detrainment occurs before destruction), convective merger will 'eventually' occur in all vortex pairs, assuming the vortices remain sufficiently strong. The onset of merging, t^*_{cr}, can be estimated by assuming viscous core growth until $(a_\omega/b)_{crit}$ is attained (as in (6.1)). In the present analysis for asymmetric pairs, we have obtained relations which enable predictions for $t^*_{cr,2}$ and $t^*_{cr,1}$ based on the determined value of γ_{cr}. However, a predictive merging criterion will be more complex, since it requires the knowledge of the vortex destruction time, $t^*_{de,2}$, and a relative comparison of the three time scales. Furthermore, $t^*_{cr,i}$ depends on $Re_{\Gamma,i}$, and since the flow evolution involves a change from diffusion-dominated to convective-dominated conditions, we may expect some Reynolds-number-dependent behaviour at low to moderate values of $Re_{\Gamma,i}$ for which diffusive and convective time scales do not widely differ. Nevertheless, our analysis provides a basis for a generalized vortex merging criterion. Further efforts are needed to demonstrate these results with additional numerical simulations, which extend the parameter range, and laboratory experiments.

The first author received support from the Achievement Rewards for College Scientists (ARCS) Foundation.

REFERENCES

Bewley, T. R. 2010 *Numerical Renaissance: Simulation, Optimization, and Control*. http://numerical-renaissance.com/Diablo.html, Renaissance.

Brandt, L. K. & Nomura, K. K. 2006 The physics of vortex merger: further insight. *Phys. Fluids* **18**, 1–4.

Brandt, L. K. & Nomura, K. K. 2007 The physics of vortex merger and the effects of ambient stable stratification. *J. Fluid Mech.* **592**, 413–446.

Cerretelli, C. & Williamson, C. H. K. 2003 The physical mechanism for vortex merging. *J. Fluid Mech.* **475**, 41–77.

Dritschel, D. G. & Waugh, D. W. 1992 Quantification of the inelastic interaction of unequal vortices in two-dimensional vortex dynamics. *Phys. Fluids* **4**, 1737–1744.

Ehrenstein, U. & Rossi, M. 1999 Equilibria of corotating non-uniform vortices. *Phys. Fluids* **11**, 3416.

Griffiths, R. W. & Hopfinger, E. J. 1987 Coalescing of geostrophic vortices. *J. Fluid Mech.* **178**, 73–97.

Huang, M. J. 2005 The physical mechanism of symmetric vortex merger: a new viewpoint. *Phys. Fluids* **17**, 1–7.

Kida, S. 1981 Motion of an elliptic vortex in a uniform shear flow. *J. Phys. Soc. Jpn* **50**, 3517.

Kimura, Y. & Herring, J. R. 2001 Gradient enhancement and filament ejection for a non-uniform elliptic vortex in two-dimensional turbulence. *J. Fluid Mech.* **439**, 43–56.

Le Dizes, S. & Verga, A. 2002 Viscous interactions of two co-rotating vortices before merging. *J. Fluid Mech.* **467**, 389–410.

Legras, B. & Dritschel, D. G. 1993 Vortex stripping and the generation of high vorticity gradients in two-dimensional flows. *Appl. Sci. Res.* **51**, 445.

Mariotti, A., Legras, B. & Dritschel, D. G. 1994 Vortex stripping and the erosion of coherent structures in two-dimension flows. *Phys. Fluids.* **120**, 1267–1297.

Melander, M. V., McWilliams, J. C. & Zabusky, N. J. 1987 Asymmetric vortex merger in two dimensions: which vortex is 'victorious'? *Phys. Fluids* **30**, 2610–2612.

Melander, M. V., Zabusky, N. J. & McWilliams, J. C. 1988 Symmetric vortex merger in two dimensions: causes and conditions. *J. Fluid Mech.* **195**, 305–340.

Meunier, P. 2001 Etude experimentale de deux tourbillons co-rotatifs. PhD dissertation, Universite d'Aix-Marseille I, France.

Meunier, P., Ehrenstein, U., Leweke, T. & Rossi, M. 2002 A merging criterion for two-dimensional co-rotating vortices. *Phys. Fluids* **14**, 2757–2766.

Meunier, P. & Leweke, T. 2001 Three-dimensional instability during vortex merging. *Phys. Fluids* **13**, 2747–2750.

Mitchell, T. B. & Driscoll, C. F. 1996 Electron vortex orbits and merger. *Phys. Fluids* **8**, 1828–1841.

Overman, E. A. & Zabusky, N. J. 1982 Evolution and merger of isolated vortex structures. *Phys. Fluids* **25**, 1297–1305.

Rossow, V. J. 1977 Convective merging of vortex cores in lift-generated wakes. *J. Aircr.* **14**, 283–290.

Saffman, P. G. & Szeto, R. 1980 Equilibrium shapes of a pair of equal uniform vortices. *Phys. Fluids* **23**, 2339–2342.

Trieling, R. R., Velasco Fuentes, O. U. & van Heijst, G. J. F. 2005 Interaction of two unequal corotating vortices. *Phys. Fluids* **17**, 1–17.

Velasco Fuentes, O. U. 2005 Vortex filamentation: its onset and its role on axisymmetrization and merger. *Dyn. Atmos. Oceans* **40**, 23–42.